Journal of Nuclear Medicine, published on August 28, 2020 as doi:10.2967/jnumed.120.250274

Multimodal imaging of two-cycle PRRT with ^{177}Lu-DOTA-JR11 and ^{177}Lu-DOTATOC in an orthotopic neuroendocrine xenograft tumor mouse model

Jakob Albrecht[1,2,3], Samantha Exner[4], Carsten Grötzinger[2,3,4], Sonal Prasad[1,5], Frank Konietschke[6,7], Nicola Beindorff[5], Anja A. Kühl[8], Vikas Prasad[1,9], Winfried Brenner[1,2,5], Eva J. Koziolek[1,2,3]

1. Charité – Universitätsmedizin Berlin, Department of Nuclear Medicine, Berlin

2. German Cancer Consortium (DKTK), Campus Berlin

3. German Cancer Research Center (DKFZ) Heidelberg, Im Neuenheimer Feld 280, 69120 Heidelberg, Germany

4. Charité – Universitätsmedizin Berlin, Department of Hepatology and Gastroenterology

5. Charité – Universitätsmedizin Berlin, Berlin Experimental Radionuclide Imaging Center (BERIC), Core Unit

6. Charité — Universitätsmedizin Berlin, Institute of Biometry and Clinical Epidemiology

7. Berlin Institute of Health (BIH), Anna-Louisa-Karsch-Straße 2, 10178 Berlin, Germany

8. Charité – Universitätsmedizin Berlin, iPATH.Berlin – Immunopathology for Experimental Models, Core Unit

9. Department of Nuclear Medicine, University Hospital Ulm, Ulm

First author: Jakob Albrecht. Augustenburger Platz 1, 13353 Berlin, Germany. Telephone: +49 30 450627828. E-mail: jakob.albrecht@charite.de

Corresponding author: Prof. Dr. Winfried Brenner. Augustenburger Platz 1, 13353 Berlin, Germany. Telephone: +49 30 450527051; Fax: +49 30 4507527051

E-mail: winfried.brenner@charite.de

Word count: 4994

Short running title: Preclinical ^{177}Lu-DOTA-JR11 assessment

Disclosure

This work was supported in part by Technologiestiftung Berlin (TSB) for NanoSPECT/CTplus use, and by Deutsche Forschungsgemeinschaft (DFG) for nanoScan PET/MRI (INST 335/454-1 FUGG) use and SFB1340 TPB06 to AAK. The authors have no conflicts of interest to declare.

ABSTRACT

Background: Peptide receptor radionuclide therapy (PRRT) using radiolabeled somatostatin receptor (SSTR) analogs is a common therapy approach in advanced neuroendocrine neoplasms (NEN). Recently, SSTR antagonists have shown promising results for imaging and therapy due to a higher number of binding sites compared with commonly used agonists. We evaluated PRRT with SSTR agonist ^{177}Lu-DOTATOC and antagonist ^{177}Lu-DOTA-JR11 longitudinally in an orthotopic murine pancreatic NEN model expressing human SSTR2. Morphologic and metabolic changes during treatment were assessed using multimodal imaging, including hybrid PET/MRI and SPECT/CT.

Methods: *In vitro* radioligand binding and internalization assays and cell cycle analysis have been performed. SSTR2-transfected BON cells (BON-SSTR2) were used for *in vivo* experiments. Tumor-bearing mice received two intravenous injections of either 100 µl saline, 30 MBq ^{177}Lu-DOTATOC or 20 MBq ^{177}Lu-DOTA-JR11 with an interval of three weeks. Weekly T2w MRI was performed for tumor monitoring. Viability of the tumor tissue was assessed by FDG-PET/MRI once after PRRT. Tumor as well as kidney uptake of the respective radiopharmaceuticals were measured 24 h after injection by SPECT/CT.

Results: ^{177}Lu-DOTA-JR11 treatment resulted in increased accumulation of cells in G2/M phase compared to ^{177}Lu-DOTATOC was observed. Animals treated with the SSTR antagonist showed a significant reduction in tumor size ($p < 0.001$) and longer median survival (207 d (IQR = 132–228)) compared to ^{177}Lu-DOTATOC (126 d (IQR = 118–129)). SPECT/CT revealed a 4-fold higher median tumor uptake for the antagonist and a 3-fold higher tumor-to-kidney ratio in the first treatment cycle. During the second therapy cycle, tumor uptake of ^{177}Lu-DOTATOC was

significantly lower (p = 0.01) while ^{177}Lu-DOTA-JR11 uptake remained stable. Imaging of tumor morphology indicated comparatively larger necrotic fractions for ^{177}Lu-DOTA-JR11 despite further tumor growth. These results were confirmed by FDG-PET, revealing the least amount of viable tumor tissue in ^{177}Lu-DOTA-JR11 treated animals with 6.2% (IQR = 2–23%).

Conclusion: ^{177}Lu-DOTA-JR11 showed a higher tumor-to-kidney ratio as well as a more pronounced cytotoxic effect in comparison to ^{177}Lu-DOTATOC. Additionally, tumor uptake was more stable over the course of two treatment cycles.

Key Words:

^{177}Lu-DOTA-JR11, multimodal imaging, PET/MRI, somatostatin receptor antagonist, peptide receptor radionuclide therapy, SPECT/CT, preclinical

INTRODUCTION

A hallmark of most neuroendocrine neoplasms (NEN) is the overexpression of somatostatin receptors (SSTR) on the tumor cell surface which has been extensively used for both diagnostic and therapeutic purposes. The current, well-established therapy is based on targeting SSTR by peptide receptor radionuclide therapy (PRRT) (*1*).

Presently, PRRT for NEN is performed with SSTR agonists primarily targeting SSTR2 such as ^{177}Lu-DOTATATE (*1,2*) or ^{177}Lu-DOTATOC, which also shows an additional low affinity for SSTR5. An improved quality of life and prolonged progression-free survival compared to non-radiolabelled SSTR analogues has been reported (*3*). In 2006, Ginj *et al.* were the first to point out the potential of SSTR antagonists for diagnostic and therapeutic purposes (*4*). SSTR antagonists recognize a higher number of receptor binding sites per cell resulting in higher tumor-to-organ ratios compared to agonists (*5-8*). In a recent biodistribution study, a tumor-to-kidney ratio of 5.4 was reported for ^{177}Lu-DOTA-JR11 compared to 3.8 for ^{177}Lu-DOTATE at 72h after injection (*8*).

So far, few preclinical and clinical studies on PRRT using the antagonist ^{177}Lu-DOTA-JR11 have been published (*8-12*). Dalm et al. showed higher tumor uptake as well as significantly more DNA double strand breaks for the SSTR antagonist *in vitro* (*9*). Longer tumor residence times and, thus, higher tumor radiation doses were reported in two clinical trials (*7,12*). However, little is known about treatment effects on the tumor itself as detectable by hybrid imaging.

The aim of this study was to compare treatment effects of two cycles of ^{177}Lu-DOTATOC and ^{177}Lu-DOTA-JR11 in NEN and provide an imaging-based tumor response analysis. Using a murine orthotopic, SSTR2-positive pancreatic NEN model, treatment response was monitored

longitudinally by multimodal imaging: tumor size and morphology by magnetic resonance imaging (MRI), radionuclide uptake by single photon emission tomography (SPECT) / computed tomography (CT) prior to and after and ^{18}F-fluoro-deoxyglucose (FDG)-positron emission tomography (PET) to provide metabolic information.

MATERIALS AND METHODS

Cell Lines

Human pancreatic BON cells, a kind gift from C. M. Townsend (University of Texas, Galveston), were grown in RPMI 1640 medium (10% fetal calf serum, 1% penicillin/ streptomycin) in a humidified atmosphere at 37°C with 5% CO_2.

Native BON cells were transfected with human SSTR2 (BON-SSTR2) (pcDNA3.1-huSSTR2, #SSTR200000, cDNA Resource Center, Bloomsberg, PA, USA; www.cdna.org) as described by Exner et al. (*13*). Stable clones were validated for SSTR2 expression by quantitative real-time PCR, immunofluorescence, and radioligand binding assay (*13*).

Radiolabeling

The precursor DOTA-JR11 was kindly provided by H. Maecke (Freiburg, Germany), and DOTATOC was purchased from ABX GmbH, Germany. $^{177}LuCl_3$ and reagent kits were purchased from ITG Isotope Technologies Garching, Germany. The radiopharmaceutical ^{177}Lu-DOTATOC was synthesized using reagent kits for ^{177}Lu manual labelling as per manufacturers' protocol. Radiolabeling of DOTA-JR11 with ^{177}Lu was performed as follows: DOTA-JR11 (25 µg) dissolved in ascorbate buffer (500 µl) was added to ^{177}LuCl3 (1 GBq) and heated for 30 min at 95°C. After

cooling to room temperature, the reaction was diluted with 1 ml of normal saline. Prior to intravenous injection, the pH of the tracer was adjusted to 6.0 using $NaHCO_3$. A reverse-phase radio-HPLC system (Knauer GmbH, Germany) was used for quality control. The radiochemical purities of ^{177}Lu-DOTATOC and ^{177}Lu-DOTA-JR11 were ≥ 99% and 95-98%, respectively. The radiochemical yields of ^{177}Lu-DOTATOC and ^{177}Lu-DOTA-JR11 were 97-99% and 90-92%, and the specific molar activities were calculated as 44-50 GBq/µmol and 21 GBq/µmol, respectively.

Binding and Internalization Assays

Peptide iodination and binding assays with iodine-labeled somatostatin were performed as previously described (*13*); for receptor competition increasing concentrations of unlabeled DOTA-TOC and DOTA-JR11 were used. Data were analyzed with GraphPad Prism 5.04 and IC_{50} values were calculated by non-linear regression (one site-fit logIC_{50}, least squares fit).

Internalization with ^{177}Lu labelled somatostatin analogs was performed as previously described (*9*).

Cell Cycle Analysis

Cell cycle analysis was performed as previously described (*13*). Cells were treated with the indicated activities of ^{177}Lu-coupled somatostatin analogs for 4 h, washed and incubated in fresh growth medium for further 20 h before analysis.

Generation of Tumor Xenograft Models

All animal experiments were performed in accordance with national and local guidelines for animal welfare and were approved by the animal ethics committee of the state Berlin (LAGeSo, Reg. No. G0011/16).

To generate the pancreatic tumor xenograft model, female severe combined immuno-deficient (SCID) mice were orthotopically inoculated with BON-SSTR2 cells. The surgery was performed under perioperative anaesthesia and analgesia ((Ketamin (0.06 mg/g) intraperitoneally, Metamizol (0.2 mg/g) and Carprofen (0.005 mg/g) subcutaneously), and inhalation anaesthesia (1-2% isoflurane/oxygen). A median laparotomy of 1-2 cm was performed and 2.0 – 2.2 x 10^6 BON-SSTR2 cells in a volume of 20 µl (serumfree RPMI1640) were inoculated directly into the pancreas tail using a 29 G syringe. To prevent leakage of tumor cells into the abdominal cavity, 0.04% polihexanid in Ringer's solution was applied to the injection site with a cotton tip.

All animals were maintained under pathogen-free conditions and were fed with sterile food and water *ad libitum*. Animal weight was monitored once a week prior to the first therapeutic injection and twice per week after therapy start.

Preliminary Study

A preliminary study was performed to evaluate the activity used for PRRT in mice as reported in current literature (*9*). Once tumors exceeded the size of 100 mm^3 animals with orthotopic pancreatic NEN received a single therapeutic intravenous (iv) injection of either 30 MBq ^{177}Lu-

DOTA-JR11 (n = 4) or ^{177}Lu-DOTATOC (n = 4). Animals were monitored weekly by T2w MRI until the tumors reached a size of 1000 mm^3 or body weight decreased by 20%.

PRRT

Each animal received two iv injections of either 30 MBq ^{177}Lu-DOTATOC (n = 4), 100 µl sterile saline (n = 4) or 20 MBq ^{177}Lu-DOTA-JR11 (n = 4), respectively. As we observed severe toxicity in our preliminary study after administration of 30 MBq 177Lu-DOTA-JR11, the activity was reduced by 30 %. ^{177}Lu-DOTATOC was used due to patent reasons of ^{177}Lu-DOTATATE. The two treatment cycles were applied within a three-week interval, starting once the tumors exceeded the size of approx. 80 mm^3. Tumors were continuously monitored as described in the following section. Animals were euthanized once the tumors reached a size of 1000 mm^3 or body weight decreased by 20%.

In Vivo Imaging

For *in vivo* PET/MRI (nanoScan PET/MRI, Mediso, Hungary) and SPECT/CT (nanoScan SPECT/CT, Mediso, Hungary) imaging, mice were anesthetized with 1-2% isoflurane/oxygen. Body temperature was kept at 37°C using a heated bed aperture and the respiration rate continuously monitored.

To assess tumor size and morphology, MRI scans were acquired using a T2-weighted (T2w) fast spin echo sequence as previously described (*14*).

In order to analyse metabolic tumor activity, FDG-PET/MRI was performed once when significant regrowth (tumor volume > 700 mm^3) was observed after the second treatment cycle.

For FDG-PET, 10 - 20 MBq FDG were administered iv 37-60 minutes prior to a 30-min acquisition. A material map for attenuation correction and additional T2w MRI were acquired.

To assess intratumoral uptake of ^{177}Lu-DOTATOC or ^{177}Lu-DOTA-JR11 during each therapy cycle, SPECT/CT was performed. A helical CT scan was acquired for anatomical orientation of the SPECT images.

Image Analysis

Interview Fusion software version 3.01 (Mediso, Hungary) was used for tumor assessment. A tumor volume of interest was drawn manually on T2w images for calculation of volumes.

PET and SPECT images were analysed with PMOD 3.505 (PMOD Technologies Ltd., Switzerland). For calculation of tumor/organ uptake, a volume of interest was placed over the whole tumor/organ on SPECT images, and the percentage tracer uptake of the injected activity per millilitre (%IA/ml) was calculated. Due to similar uptakes of left and right kidneys, a mean value was calculated for both.

Metabolically active tumor tissue was determined by fused FDG-PET and T2w MRI as previously described (*15*). Briefly, a tumor volume of interest was placed onto T2w images (Vol_{tumor}). FDG-avid tumor was automatically delineated by PMOD, using a threshold of 30% of the maximum activity within the Vol_{tumor}. Viable tumor was defined as the FDG-avid portion of the whole tumor volume as delineated in T2w images.

Histopathology

Paraffin sections of tumor tissues were de-paraffinized and stained with hematoxylin (Merck) and eosin (Sigma-Aldrich) as described elsewhere (*16*).

Statistics

Tumor growth delay was defined as the difference in time to reach a tumor volume of 1000 mm^3 between the treatment and control groups as previously described (*9*). Linear interpolation was performed in MATLAB R2018a (Mathworks) to calculate the median tumor sizes per time point for each group. Due to the rather small sample sizes, approximate statistical methods for the analysis of factorial longitudinal data (repeated measures designs) with factors ‘’group” and “time” were used (*17*) . The methods are implemented in the *R package (www.r-project.org) MANOVA.RM* (*18*). For size comparison, both semi-parametric (MANOVA.RM) and purely non-parametric (nparLD) (*19*) approaches for repeated measure design were applied. All statistical analysis was performed using R software (version 3.6.1) at 5% level of significance. Due to the very small sample sizes, p-values are interpreted in an exploratory supplementary manner.

RESULTS

In Vitro

For assessing the therapeutic effects of ^{177}Lu-DOTATOC and ^{177}Lu-DOTA-JR11 *in vitro*, both tracers were applied to BON-SSTR2 cells. Strong binding was demonstrated for both tracers in a radioligand competition assay, and iodine-labeled somatostatin was displaced dose-dependently by unlabeled DOTATOC (IC_{50} = 13.1 nM) and DOTA-JR11 (IC_{50} = 2.3 nM), revealing a

6-fold higher affinity for the SSTR antagonist. Native BON cells reached background levels of binding only (Fig. 1A). Interestingly, the activity bound to BON-SSTR2 cells was up to 10-fold higher for antagonistic ^{177}Lu-DOTA-JR11 when compared to agonistic ^{177}-Lu-DOTATOC. The largest fraction of the antagonist was membrane-bound (80 % of cell-bound activity), while 80 % of the agonist was internalized. As expected, native BON cells demonstrated only little binding with no displacement (Fig. 1B).

For assessment of radiation effects on BON-SSTR2 cell proliferation, the cell cycle distribution after incubation with either radiopeptide was analyzed. Cell cycle phases remained unchanged in both BON-SSTR2 and BON cells after treatment with 0.1 or 1.0 MBq ^{177}Lu-DOTATOC. In contrast, ^{177}Lu-DOTA-JR11 induced an increasing accumulation of BON-SSTR2 cells in G2/M from 23 % (control) to 38 % (0.1 MBq) and 63 % (1.0 MBq). This was mirrored by a decreased proportion of cells in G0/G1 phase (57 % vs 43 % (0.1 MBq) or 17 % (1.0 MBq)). Native BON cells showed no change in cell cycle phases (Fig. 1C).

Preliminary Study

All animals receiving 30 MBq ^{177}Lu-DOTA-JR11 died within three weeks after PRRT, indicating severe toxicity of the administered activity. A significant weight loss was observed prior to death. Dissection postmortem did not reveal any signs of internal bleeding, infection, or other obvious causes of death.

^{177}Lu-DOTATOC treated animals tolerated the activity of 30 MBq well, and T2w MRI revealed a stable tumor size for three weeks (Supplemental Figure 1) before tumor regrowth.

In Vivo Imaging

For both, ^{177}Lu-DOTATOC and ^{177}Lu-DOTA-JR11 treated animals, significant growth differences were found compared to the saline treatment group on day 20 ($p < 0.001$) and day 35 ($p < 0.001$). Following the first treatment cycle with ^{177}Lu-DOTA-JR11, tumors showed a continuous decrease in tumor size for 27 d (IQR = 20 - 56). In ^{177}Lu-DOTATOC treated animals, tumors showed a decreased growth rate but no decrease in volume (Fig. 2A). One out of 4 animals in the ^{177}Lu-DOTA-JR11 group died unexpectedly after 111 d (tumor size 125 mm^3) and was withdrawn from the growth curve.

Kaplan-Meyer analysis (Fig. 2B) revealed the longest survival and growth delay for ^{177}Lu-DOTA-JR11 treated animals (Table 1).

Visual assessment of the T2w MRI revealed increasing fractions of non-viable (hypointense) tumor tissue over time in all three groups (Fig. 3A). After the second PRRT cycle, ^{177}Lu-DOTATOC treated tumors showed no relevant changes in morphology, but rather remained in a stable state. In contrast, ^{177}Lu-DOTA-JR11 treated animals revealed a significant loss of overall tumor mass, with almost no viable tumor tissue three weeks after PRRT. Subsequently, regrowth occurred in all treatment groups, pronounced at the tumor rim. To confirm glucose metabolism as a biomarker for viability of the regrowing tissue, FDG-PET was performed once tumors reached a size of at least 700 mm^3. PET analysis showed that the hyperintense tumor areas relate to metabolically active tissue revealing a median viable tumor volume after the second therapy cycle of 24.1 % (IQR = 16 - 40) for ^{177}Lu-DOTATOC and 6.2 % (IQR = 2 - 23) for ^{177}Lu-DOTA-JR11 (Figs. 3 B and C). The control group showed the largest fraction of viable tumor tissue in FDG-PET analysis (median = 46.4 % (IQR = 35 – 56)). Post mortem H&E staining

confirmed varying amounts of necrotic tissue between tumor center and rim (Fig. 4A), showing more viable tissue in the tumor rim.

SPECT/CT imaging 24 h after each therapy cycle showed a 4 – 6-fold higher median tumor uptake as well as a 3 – 5-fold higher tumor-to-kidney-ratio for ^{177}Lu-DOTA-JR11 than for the SSTR agonist DOTATOC (Supplemental Figure 2). While ^{177}Lu-DOTATOC showed a decreased uptake during the second cycle ($p = 0.01$) descriptive data indicate an increasing uptake for ^{177}Lu-DOTA-JR11 ($p = 0.1$). Kidney uptakes showed no significant differences between the treatment groups or therapy cycles (Table 2)

DISCUSSION

PRRT with the receptor agonist ^{177}Lu-DOTATATE is a standard FDA and EMA approved treatment regimen in patients with metastatic NEN. Novel SSTR antagonists such as ^{177}Lu-DOTA-JR11 have recently shown potential benefit over SSTR agonists for PRRT. In this study, we analysed morphologic and metabolic treatment efficacy of two subsequent PRRT cycles with the SSTR antagonist ^{177}Lu-DOTA-JR11 in comparison to the receptor agonist ^{177}Lu-DOTATOC over time in an orthotopic NEN tumor mouse model by SPECT, PET and MRI.

Although the antagonist DOTA-JR11 showed a much lower internalization rate of only 20% of the cell-bound activity *in vitro*, and thus a higher radiation distance to the nucleus, ^{177}Lu-DOTA-JR11 caused an activity-dependent increase of tumor cell accumulation in the G2/M phase and a decreased fraction of cells in the G0/G1 phase compared to the control group while the same amount of radioactivity of ^{177}Lu-DOTATOC did not affect the cell cycle. A possible explanation for this interesting and clinically relevant observation is, that the antagonistic ligand DOTA-JR11

revealed a 6-fold higher affinity for SSTR and 10-fold higher activity bound to BON-SSTR2 tumor cells compared to DOTATOC which resulted in a measurable, favorable therapeutic effect of G2/M cell cycle arrest (Fig. 1). These promising data are in line with previously published results on SSTR2 transfected U2OS cells by Dalm et al. who reported an increased number of DNA double strand breaks for antagonists (*9*).

In vivo, a significant tumor volume reduction was observed only after ^{177}Lu-DOTA-JR11 treatment (Fig. 2A). This is partially in line with the findings of Dalm et al. who reported a decrease in tumor size for both radiopharmaceuticals, with a greater decrease in SSTR antagonist treated animals (*9*). Additionally, we found increasing fractions of hypointense tissue within the tumors (Fig. 3A), most likely consisting of necrotic or apoptotic cells (*20*). As such effects are seen in all treatment groups, one possible explanation is the fast growth rate of the tumors and thus, a consecutive lack of center perfusion. Since central necrosis is more pronounced in PRRT treated tumors and regrowth was primarily observed at the rim, relatively higher radiation doses in the tumor center, as described by Champion et al. (*21*), may also play a role to explain our observation.

This effect was particularly pronounced in ^{177}Lu-DOTA-JR11 treated animals, and correlating FDG-PET images revealed the least amount of metabolically active tumor tissue (Fig. 3B and C). Hence, these findings indicate - in addition to the overall reduction of tumor mass - a greater destruction of viable tumor tissue by ^{177}Lu-DOTA-JR11, independent of the apparent tumor size. Tumor volume reduction, e.g. by chemotherapy or PRRT, is a valuable tool to prepare advanced but potentially resectable NEN for curative surgery (*22*). The more pronounced and distinct cytoreductive effect of ^{177}Lu-DOTA-JR11 in comparison to ^{177}Lu-DOTATOC therefore may be of

great interest for using PRRT as a neoadjuvant tool in NEN therapy.

The growth delay in our study was significantly longer than previously reported (*9*). These differences may be explained by various factors: 1) A second therapy cycle. Baum *et al.* reported longer progression free survival for patients receiving more than one PRRT cycle of ^{177}Lu-DOTATOC (*23*). 2) The lower number of cells injected in our study (2–2.2 x 10^6 vs 4–40 x 10^6), resulting in an overall reduced pace of tumor growth. 3) The different growth curve of SCLC cell line H69 compared to SSTR2 transfected BON cells and 4) the different tumor locations (orthotopic vs. subcutaneous). Orthotopic tumor models are known to present a different physiology, e.g. higher vascular density and perfusion (*24*). These characteristics result in higher accessibility of the tumor for drugs and may translate into longer tumor growth delay.

Tumor and kidney uptakes of the respective radiopharmaceuticals were monitored by SPECT imaging during each therapy cycle. While the uptake of ^{177}Lu-DOTA-JR11 remained stable or even increased over the course of two PRRT cycles, ^{177}Lu-DOTATOC uptake significantly decreased (Table 2). While kidney uptakes showed no different uptake during the second treatment cycle, an increased tumor-to-kidney-ratio was calculated for ^{177}Lu-DOTA-JR11 for the second treatment cycle. In comparison, the tumor-to-kidney-ratio in the ^{177}Lu-DOTATOC group decreased (Supplemental Figure 2). Since renal failure is an important therapy limiting factor (*25*), high tumor-to-kidney ratios are favorable to successfully treat tumors without major kidney toxicity. Wild et al. reported a 6.2-fold higher tumor-to-kidney ratio for the SSTR antagonist ^{177}Lu-DOTA-JR11 compared to ^{177}Lu-DOTATATE in a clinical trial (*7*). The overall lower tumor-to-kidney ratios reported in our study may result from the lack of nephroprotection. Beykan et al. found a 2-fold increased kidney uptake of ^{177}Lu-DOTA-JR11 when no renal

protection was applied (*10*). It must be mentioned though, that DOTATATE and DOTATOC have different SSTR2 affinities *in vitro* and, thus, are not directly comparable. Nevertheless, the data presented here confirm the favorable role of ^{177}Lu-DOTA-JR11 in reducing renal radiation exposure during PRRT in NEN.

In our preliminary study, all animals died after administration of 30 MBq ^{177}Lu-DOTA-JR11 and thus, the activity was reduced by 30%. As the bone marrow is also discussed to be a therapy limiting factor (*8*), a possible explanation is a hematotoxic effect. Reidy-Lagunes et al. reported increased grade 4 hematologic toxicity after one and two PRRT cycles using ^{177}Lu-Satoreotide Tetraxetane (JR11). After reducing the amount of ^{177}Lu by 50%, no patients developed hematotoxicity (*12*). Even though we cannot retrospectively evaluate the reason for premature death of the animals in our preliminary study, as we didn't take blood samples, the administered activity in future studies and the respective toxic effects to organs should be evaluated carefully.

One limiting factor of the present study is the small sample size. Due to time consuming multimodal imaging and tracer availability, we had to limit the number of animals and imaging sessions in order to guarantee the feasibility of such long-term study.

CONCLUSION

We showed a pronounced cytotoxic treatment effect for the SSTR antagonist ^{177}Lu-DOTA-JR11 in comparison to the standard agonistic ^{177}Lu-DOTATOC, leading to significant reduction of viable tumor tissue, a more pronounced tumor growth delay and a longer survival *in vivo* and a higher accumulation of cells in the vulnerable G2/M cell cycle phase *in vitro*. Over the course of

two PRRT cycles, SPECT/CT imaging revealed an approximately 4-fold higher tumor uptake, which remained high during the second cycle of treatment, as well as a more favorable tumor-to-kidney ratio compared to ^{177}Lu-DOTATOC.

DISCLOSURE

This work was supported in part by Technologiestiftung Berlin (TSB) for NanoSPECT/CTplus use, and by Deutsche Forschungsgemeinschaft (DFG) for nanoScan PET/MRI (INST 335/454-1 FUGG) use and SFB1340 TPB06 to AAK. The authors have no conflicts of interest to declare.

ACKNOWLEDGMENTS

The authors thank Janpeter Hirsch for assistance with data processing, Fränze Schmidt for helping with PET/MRI measurements, Dietrich Polenz for support in establishing the animal model, Prof. H. Maecke (University Hospital Freiburg, Germany) for providing the precursor DOTA-JR11, and Prof. C. M. Townsend, Jr. (University of Texas, Galveston) for providing the human pancreatic BON cells.

KEY POINTS

Question: Does ^{177}Lu-DOTA-JR11 show favorable treatment effects for PRRT in NEN compared to ^{177}Lu-DOTATOC?

Pertinent finding: In an orthotopic mouse model, ^{177}Lu-DOTA-JR11 showed a higher therapeutic effect and more favorable tumor-to-kidney ratio.

Implications for patient care: ^{177}Lu-DOTA-JR11 is a promising radiopharmaceutical for advanced NEN.

REFERENCES

1. Pavel M, O'Toole D, Costa F, et al. ENETS Consensus Guidelines Update for the Management of Distant Metastatic Disease of Intestinal, Pancreatic, Bronchial Neuroendocrine Neoplasms (NEN) and NEN of Unknown Primary Site. *Neuroendocrinology.* 2016;103:172-185.

2. Falconi M, Eriksson B, Kaltsas G, et al. ENETS Consensus Guidelines Update for the Management of Patients with Functional Pancreatic Neuroendocrine Tumors and Non-Functional Pancreatic Neuroendocrine Tumors. *Neuroendocrinology.* 2016;103:153-171.

3. Strosberg J, El-Haddad G, Wolin E, et al. Phase 3 Trial of (177)Lu-Dotatate for Midgut Neuroendocrine Tumors. *N Engl J Med.* 2017;376:125-135.

4. Ginj M, Zhang H, Waser B, et al. Radiolabeled somatostatin receptor antagonists are preferable to agonists for in vivo peptide receptor targeting of tumors. *Proc Natl Acad Sci U S A.* 2006;103:16436-16441.

5. Fani M, Braun F, Waser B, et al. Unexpected sensitivity of sst2 antagonists to N-terminal radiometal modifications. *J Nucl Med.* 2012;53:1481-1489.

6. Wild D, Fani M, Behe M, et al. First clinical evidence that imaging with somatostatin receptor antagonists is feasible. *J Nucl Med.* 2011;52:1412-1417.

7. Wild D, Fani M, Fischer R, et al. Comparison of somatostatin receptor agonist and antagonist for peptide receptor radionuclide therapy: a pilot study. *J Nucl Med.* 2014;55:1248-1252.

8. Nicolas GP, Mansi R, McDougall L, et al. Biodistribution, Pharmacokinetics, and Dosimetry of (177)Lu-, (90)Y-, and (111)In-Labeled Somatostatin Receptor Antagonist OPS201 in Comparison to the Agonist (177)Lu-DOTATATE: The Mass Effect. *J Nucl Med.* 2017;58:1435-1441.

9. Dalm SU, Nonnekens J, Doeswijk GN, et al. Comparison of the Therapeutic Response to Treatment with a 177Lu-Labeled Somatostatin Receptor Agonist and Antagonist in Preclinical Models. *J Nucl Med.* 2016;57:260-265.

10. Beykan S, Dam JS, Eberlein U, et al. (177)Lu-OPS201 targeting somatostatin receptors: in vivo biodistribution and dosimetry in a pig model. *EJNMMI Res.* 2016;6:50.

11. Beykan S, Fani M, Jensen SB, et al. In Vivo Biokinetics of (177)Lu-OPS201 in Mice and Pigs as a Model for Predicting Human Dosimetry. *Contrast Media Mol Imaging.* 2019;2019:6438196.

12. Reidy-Lagunes D, Pandit-Taskar N, O'Donoghue JA, et al. Phase I Trial of Well-Differentiated Neuroendocrine Tumors (NETs) with Radiolabeled Somatostatin Antagonist (177)Lu-Satoreotide Tetraxetan. *Clin Cancer Res.* 2019;25:6939-6947.

13. Exner S, Prasad V, Wiedenmann B, Grotzinger C. Octreotide Does Not Inhibit Proliferation in Five Neuroendocrine Tumor Cell Lines. *Front Endocrinol (Lausanne).* 2018;9:146.

14. Erdmann S, Niederstadt L, Koziolek EJ, et al. CMKLR1-targeting peptide tracers for PET/MR imaging of breast cancer. *Theranostics.* 2019;9:6719-6733.

15. Albrecht J, Polenz D, Kuhl AA, et al. Diffusion-weighted magnetic resonance imaging using a preclinical 1 T PET/MRI in healthy and tumor-bearing rats. *EJNMMI Res.* 2019;9:21.

16. Erben U, Loddenkemper, C. Spieckermann, S., Heimesaat, M.M., Siegmund, B., Kühl, A.A. Histomorphology of intestinal inflammation in inflammatory bowel diseases (IBD) mouse models and its relevance for IBD in men. *Int J Clin Exp Pathol.* 2016;9:35.

17. Friedrich S, Brunner E, Pauly M. Permuting longitudinal data in spite of the dependencies. *Journal of Multivariate Analysis.* 2017;153:255-265.

18. Friedrich S, Konietschke F, Pauly M. Analysis of Multivariate Data and Repeated Measures Designs with the R Package MANOVA.RM. 2018.

19. Noguchi K, Gel Y, Brunner E, Konietschke F. nparLD: An R Software Package for the Nonparametric Analysis of Longitudinal Data in Factorial Experiments. *Journal of Statistical Software.* 2012;50.

20. Jardim-Perassi BV, Huang S, Dominguez-Viqueira W, et al. Multiparametric MRI and Coregistered Histology Identify Tumor Habitats in Breast Cancer Mouse Models. *Cancer Res.* 2019;79:3952-3964.

21. Champion C, Zanotti-Fregonara P, Hindie E. CELLDOSE: a Monte Carlo code to assess electron dose distribution--S values for 131I in spheres of various sizes. *J Nucl Med.* 2008;49:151-157.

22. Pozzari M, Maisonneuve P, Spada F, et al. Systemic therapies in patients with advanced well-differentiated pancreatic neuroendocrine tumors (PanNETs): When cytoreduction is the aim. A critical review with meta-analysis. *Cancer Treat Rev.* 2018;71:39-46.

23. Baum RP, Kluge AW, Kulkarni H, et al. [(177)Lu-DOTA](0)-D-Phe(1)-Tyr(3)-Octreotide ((177)Lu-DOTATOC) For Peptide Receptor Radiotherapy in Patients with Advanced Neuroendocrine Tumours: A Phase-II Study. *Theranostics.* 2016;6:501-510.

24. Ho KS, Poon PC, Owen SC, Shoichet MS. Blood vessel hyperpermeability and pathophysiology in human tumour xenograft models of breast cancer: a comparison of ectopic and orthotopic tumours. *BMC Cancer.* 2012;12:579.

25. van Essen M, Krenning EP, Kam BL, de Jong M, Valkema R, Kwekkeboom DJ. Peptide-receptor radionuclide therapy for endocrine tumors. *Nat Rev Endocrinol.* 2009;5:382-393.

Table 1. Median survival in all three treatment groups.

treatment	**median survival [d] (IQR)**	**median growth delay* [d] (IQR)**
saline	80 (72 – 84)	-
^{177}Lu-DOTATOC	126 (118 – 129)	46 (38 – 49)
^{177}Lu-DOTA-JR11	207 (132 – 228)	141 (113 – 150)

* compared to saline treated animals

Table 2. Median uptake of ^{177}Lu-DOTATOC and ^{177}Lu-DOTA-JR11 24 hours after injection.

treatment	**1. PRRT cycle**		**2. PRRT cycle**	
	tumor [%IA/ml] (IQR)	**kidney [%IA/ml] (IQR)**	**tumor [%IA/ml] (IQR)**	**kidney [%IA/ml] (IQR)**
^{177}Lu-DOTATOC	2.7 (2.4 – 2.9)	2.6 (2.0 – 2.7)	2.0 (1.8 – 2.3)	2.5 (2.3 – 4.2)
^{177}Lu-DOTA-JR11	10.4 (9.3 – 10.9)	3.2 (2.8 – 3.6)	12.9 (9.9 – 14.0)	3.0 (2.9 – 3.5)

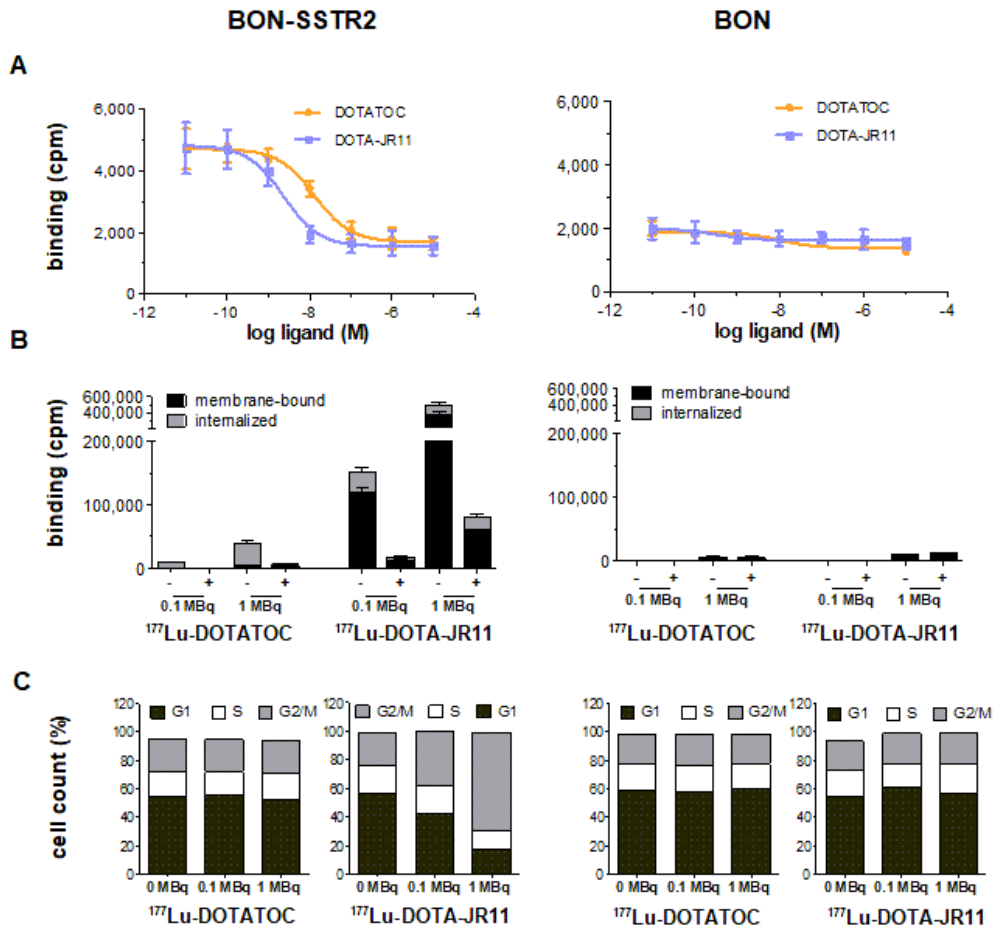

Figure 1. (A): SSTR2-transfected (left column) and native BON (right column) cells were incubated with iodine-125 labeled Tyr_{11}-somatostatin-14 and increasing concentrations of unlabeled DOTATOC or DOTA-JR11 (± S.E.M.;n = 3 each). (B): The respective cell lines were incubated with different doses of ^{177}Lu-DOTATOC or ^{177}Lu-DOTA-JR11. Resulting membrane-bound and internalized fractions in absence (-) or presence (+) of 1 µM unlabeled octreotide are presented (mean ± S.E.M.;n = 2-3). (C): Cell cycle distribution depicting the percentage of cells in each phase (n = 1). cpm, counts per minute; MBq, megabecquerel

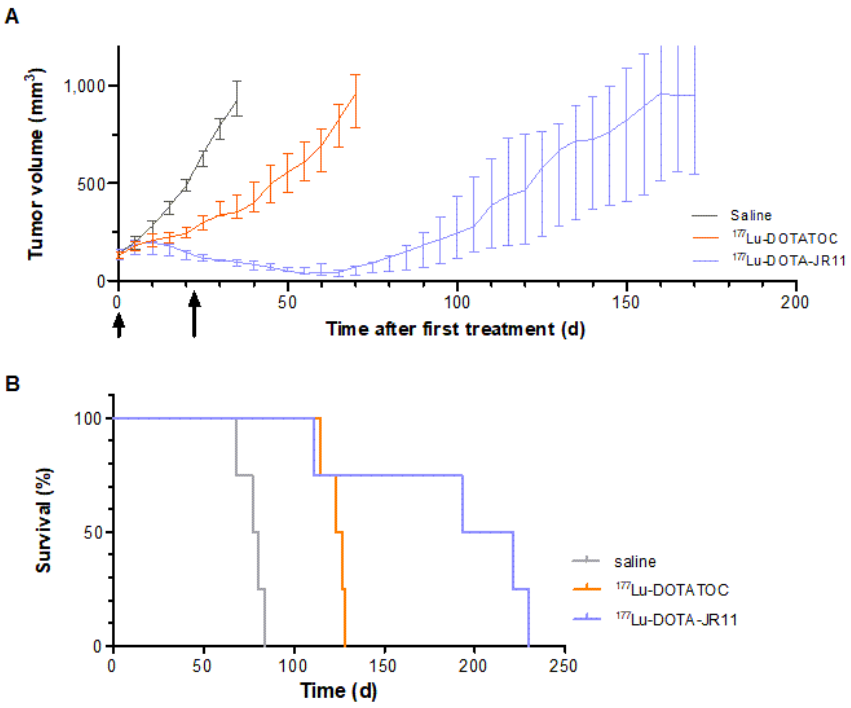

Figure 2. In vivo data of an orthotopic, pancreatic SSTR2-positive NEN model. (A): 3-week interval PRRT (2 cycle): Animals received two injections (arrows) of either 100 µl saline (n = 4), 30 MBq ^{177}Lu-DOTATOC (n = 4) or 20 MBq ^{177}Lu-DOTA-JR11 (n = 4). Tumor growth was monitored until tumors reached a volume of 1000 mm^3 or animals dropped out for other reasons. (B) Corresponding Kaplan-Meyer survival curves.

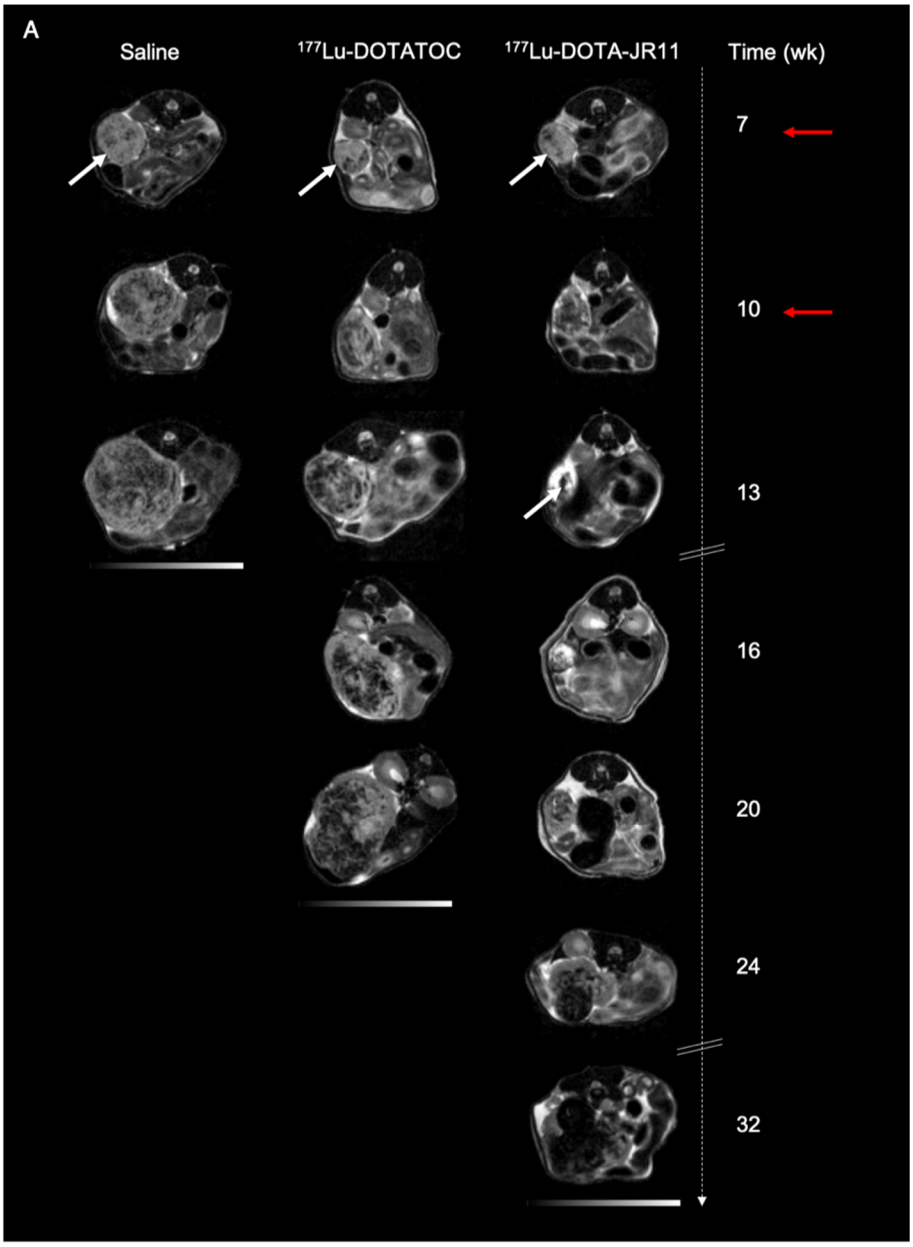
A
Saline
177Lu-DOTATOC
177Lu-DOTA-JR11
Time (wk)
7
10
13
16
20
24
32

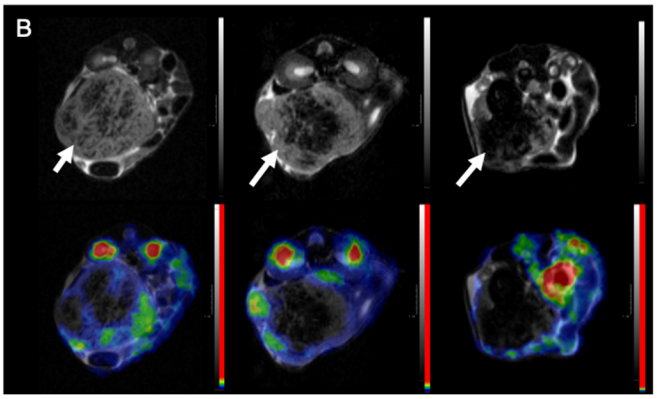
B

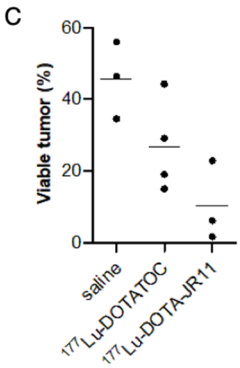
C
Viable tumor (%)
60
40
20
0
saline
177Lu-DOTATOC
177Lu-DOTA-JR11

Figure 3. Tumor tissue monitoring over time: (A) Representative axial T2w MRI of orthotopic tumors (white arrow) for the different treatment regimens. Animals received two injections (red arrows) of either 100 µl saline, 30 MBq ^{177}Lu-DOTATOC or 20 MBq ^{177}Lu-DOTA-JR11. Tumor tissue appears rather hyperintense, while the increasing portion of non-viable, e.g. necrotic, tissue appears hypointense. (B) Corresponding T2w MRI (upper row) and fused FDG-PET/MRI (lower row) shows metabolically active regions within the tumor. (C) Dot plot representing viable tumor volume and mean values (horizontal line).

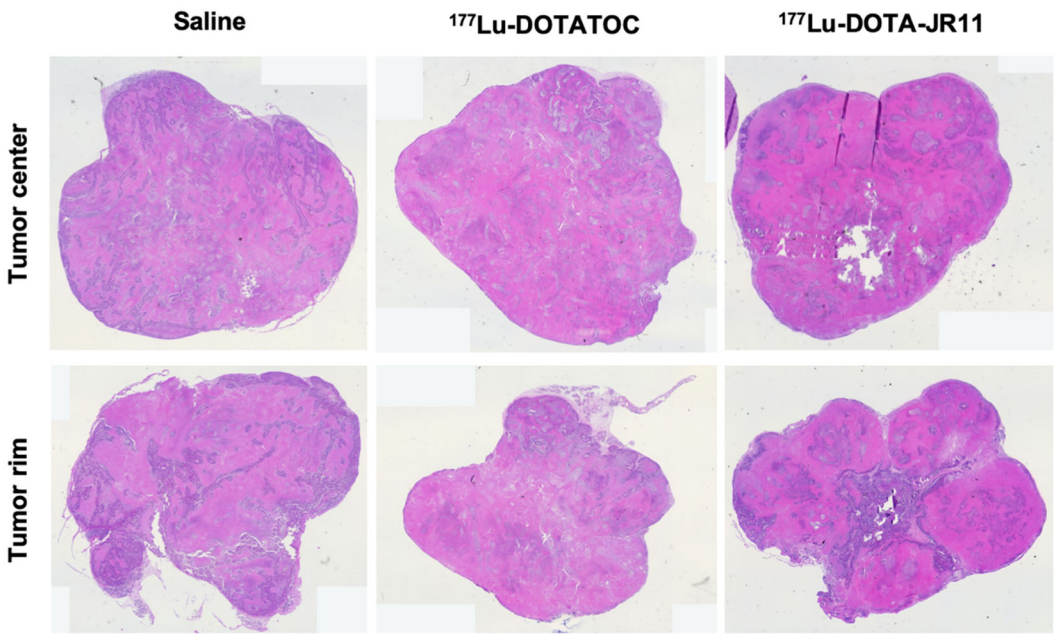

Figure 4. Immunohistochemistry of tumor tissue cross sections: Hematoxylin and eosin staining showing different amounts of necrosis between tumor rim and center.

Multimodal imaging of two-cycle PRRT with ^{177}Lu-DOTA-JR11 and ^{177}Lu-DOTATOC in an orthotopic neuroendocrine xenograft tumor mouse model

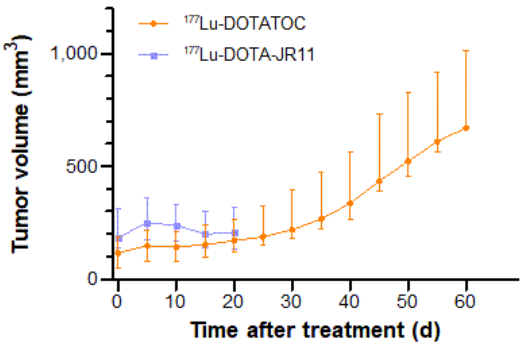

Supplemental Figure 1. Tumor growth curve of the one-cycle PRRT preliminary study after a single iv injection of either 30 MBq ^{177}Lu-DOTATOC (n = 4) or ^{177}Lu-DOTA-JR11 (n = 4). Data represent the median tumor volumes and interquartile ranges. PRRT, peptide receptor radionuclide therapy.

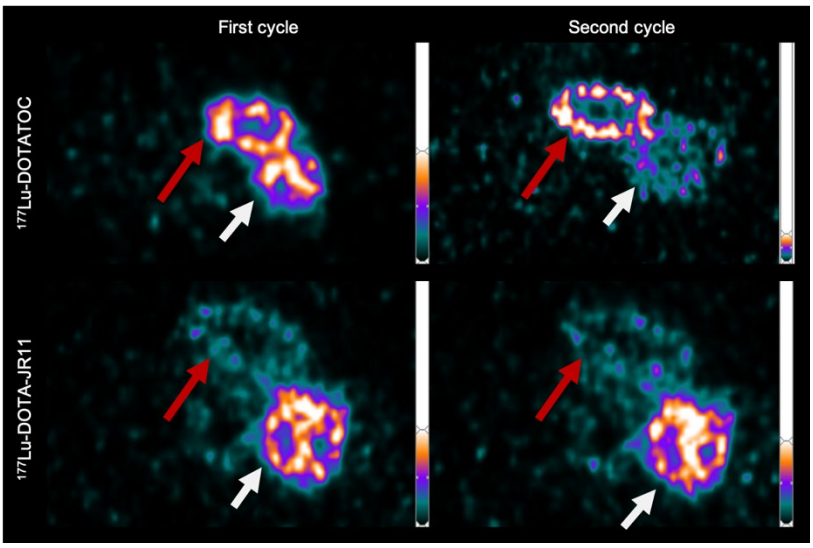

Supplemental Figure 2. SPECT measurements 24 h after i.v. injection of either 20 MBq ^{177}Lu-DOTA-JR11 (SSTR antagonist) or 30 MBq ^{177}Lu-DOTATOC (SSTR agonist) for two therapy cycles. The images represent the uptake of the respective radiopharamaceutical into the tumor (white arrow) and kidneys (red arrow), indicating a higher tumor-to-kidney-ratio for the SSTR antagonist. MBq, megabecquerel; SSTR, somatostatin receptor.